Scalable Computing: Practice and Experience, ISSN 1895-1767, http://www.scpe.org
© 2025 SCPE. Volume 26, Issues 2, pp. 829–836, DOI 10.12694/scpe.v26i2.4020

THE CASTING PROCESS OPTIMIZATION AND MELT FLOW SIMULATION BASED ON COMPUTER SIMULATION AND DATA MINING

YI DING*, XINGANG SONG†, AND DONGMING ZHANG‡

Abstract. The flow state and velocity of magnesium alloy melt at different temperatures were studied by a contact test method. Using the SOLA-VOF finite difference method, the mathematical model of the three-dimensional flow field and temperature field in the flow field of magnesium alloy twin-roll casting-rolling molding stand plate was established. The liquid magnesium alloy melt takes the form of a convex arc and advances successively on the liquid metal surface. This is mainly due to the mass accumulation of the pyrolytic products in the liquid magnesium alloy melt. The filling time is shortened with the increase of pouring temperature and vacuum degree. In the filling stage, the filling rate showed periodic alternating changes.

Key words: Lost mold casting; Magnesium alloy; Melt flow; Flow velocity; Computer simulation

1. Introduction. Compared with conventional sand casting, evaporative mold filling involves many physical and chemical problems, such as heat transfer, filling flow, chemical reaction and cooling solidification. A specific coupling effect between the above factors leads to the liquid metal filling becoming more complicated. This has a significant impact on the quality of the casting products. In liquid metal filling, evaporation mold vaporization will consume most heat energy, resulting in a sharp drop in its front temperature [1]. The combined effect of the evaporation rate and the return of the pyrolysis product leads to a significant decrease in the flow performance of the melt. This is prone to problems such as cold isolation and insufficient pouring [2]. Achieving a uniform and continuous flow field structure is a critical way to reduce defects such as porosity in castings [3]. Therefore, the research on this problem has been widely concerned by people.

The melting points of magnesium and aluminum are very close, and the casting temperatures are very different [4]. Because the latent heat of crystallization of magnesium alloy is lower than that of aluminum alloy, and it is easy to oxidize, the casting temperature is difficult to be too high. This results in rapid solidification and transient liquid phase retention of the magnesium alloy, resulting in poor workability and increased shrinkage defects related to the plastic deformation of the alloy. In addition, since magnesium alloys have a lighter mass than aluminum alloys, the processing efficiency is also lower [5]. At a certain altitude, the static pressure head weakens the filling, while the negative pressure plays a more significant role. Therefore, completely copying the filling rules of aluminum alloy does not apply to magnesium alloy technology.

In addition to using photographic technology for some exploratory research, there are almost no other research results. The photographic method is a direct measurement method, but because it is impervious to water, its cooling performance differs significantly from loose sand [6]. This results in a significant difference between the measured and measured values. The electric contact method measured the filling process of magnesium alloy liquid in a lost mold [7]. The effect of vacuum degree and pouring temperature on the filling behavior of magnesium alloy melt was studied. This provides a theoretical basis for the further preparation of magnesium alloy melt.

2. Test method and device. The influence of pouring temperature, vacuum degree and gate number on the melt flow state was studied. The rheological properties of polymer foamed plastic mold were studied [8]. The pattern density is 0.020g/cm3. The shape and size of the flat sample and the internal gate are shown in

*College of Mechanical and Electronic Engineering, Huanghe Jiaotong University, Jiaozuo Henan 454950, China (Corresponding author, 15890129126@163.com)
†College of Mechanical and Electronic Engineering, Huanghe Jiaotong University, Jiaozuo Henan 454950, China
‡College of Mechanical and Electronic Engineering, Huanghe Jiaotong University, Jiaozuo Henan 454950, China

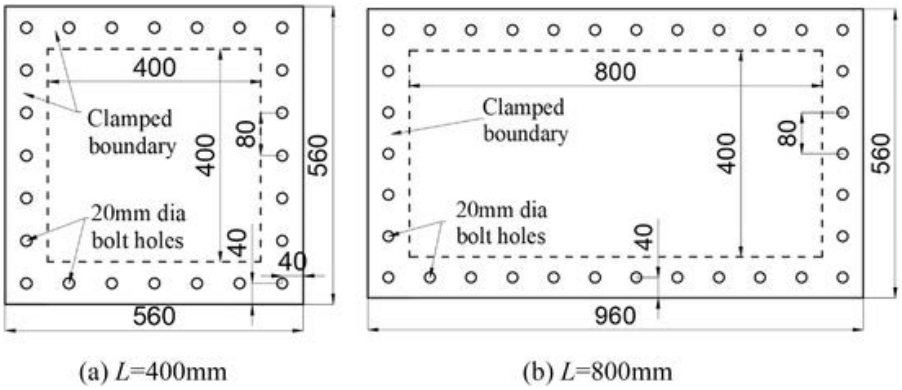

Fig. 2.1: *Shape and size of foam board sample for test.*

Fig. 2.1. The model is divided into single disc and double disc. Both are 10 mm thick. The "+" on the disk indicates electrical contact insertion [9]. The size of the straight gate used in the experiment was 30 mm X30 mm x240 mm, while the size of the cross gate was 30 mm x25 mm x 55 mm.

The influence of different process conditions on the filling morphology of magnesium solution was studied using a contact filling test device. In the test process, the appearance and the pouring parts are bonded by hot melt adhesive, and then the module is painted and baked in the oven [10]. The temperature of the oven should not exceed 50℃. The dried module is placed in the reverse sandbox and filled with water to wash the quartz sand. Vibrate on a three-dimensional vibratory compaction platform and cover with plastic film. Please turn on the vacuum pump so that it is in a stable state. Then, perfusion was performed and lasted for 5 minutes after the end of perfusion [11]. The magnesium alloy ingot is melted in a crucible resistance furnace with a capacity of 5 kg and a power of 5 kW. Flux is used in smelting. When all the charge is melted, the temperature is adjusted to 740-760 degrees, then hexachlorophene is added to remove steam; after refining, stop for 15-20 min, then adjust it to the required temperature and pour.

3. Numerical simulation of flow and temperature field in casting furnace.

3.1. System Assumptions.

1. Magnesium alloy is an exemplary flow material. Magnesium metal liquid is regarded as a continuous incompressible Newtonian fluid during simulation.
2. The apparent viscosity of the liquid magnesium fluid between the liquidus and the solid phase is set as a temperature-dependent model and in a straight-line manner.
3. The numerical calculation is based on the flow diversion mode inside the gate, and the line segment from the liquid outlet end of the gate to the middle of the roll gap is simplified into the overall flow zone with the inner side of the gate [12]. The surrounding materials are all adiabatic, so the temperature change of the liquid steel during the casting and rolling process is ignored, and only the uniformity of the temperature field in the flow zone is concerned.

3.2. Governing Equation. The SOLA-VOF method was used to calculate the difference in magnesium alloy melt flow in the cast, and the following formula was obtained: Continuity equation:

$$\frac{\partial \alpha}{\partial x}+\frac{\partial \beta}{\partial y}+\frac{\partial \gamma}{\partial z}=0 \tag{3.1}$$

Momentum conservation equation:

$$\begin{aligned}
&\frac{\partial \alpha}{\partial t}+\alpha\frac{\partial \alpha}{\partial x}+\beta\frac{\partial \alpha}{\partial y}+\gamma\frac{\partial \alpha}{\partial z}=-\frac{1}{\rho}\frac{\partial p}{\partial x}+g_x+\delta\left(\frac{\partial^2 \alpha}{\partial x^2}+\frac{\partial^2 \alpha}{\partial y^2}+\frac{\partial^2 \alpha}{\partial z^2}\right)\\
&\frac{\partial \beta}{\partial t}+\alpha\frac{\partial \beta}{\partial x}+\beta\frac{\partial \beta}{\partial y}+\gamma\frac{\partial \beta}{\partial z}=-\frac{1}{\rho}\frac{\partial p}{\partial y}+g_y+\delta\left(\frac{\partial^2 \beta}{\partial x^2}+\frac{\partial^2 \beta}{\partial y^2}+\frac{\partial^2 \beta}{\partial z^2}\right)
\end{aligned} \tag{3.2}$$

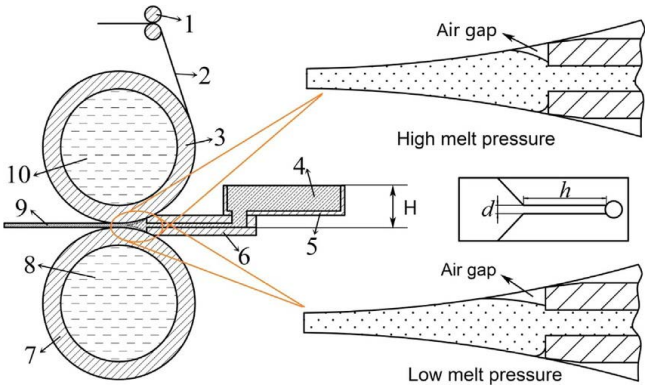

Fig. 3.1: *Schematic diagram of flow field of molten steel from box to gate and roll gap center line during casting and rolling .*

$$\frac{\partial \gamma}{\partial t} + \alpha \frac{\partial \gamma}{\partial x} + \beta \frac{\partial \gamma}{\partial y} + \gamma \frac{\partial \gamma}{\partial z} = -\frac{1}{\rho}\frac{\partial p}{\partial z} + g_z + \delta \left(\frac{\partial^2 \gamma}{\partial x^2} + \frac{\partial^2 \gamma}{\partial y^2} + \frac{\partial^2 \gamma}{\partial z^2} \right) \tag{3.3}$$

α, β, γ is the velocity vector of x, y, z in the coordinate system, and p is the pressure; Where ρ represents the concentration of magnesium alloy liquid, g_x, g_y, g_z represents gravitational acceleration, and δ represents dynamic viscosity. When using the volumetric function method to track the free surface motion, the H-type equation must also be solved:

$$\frac{\partial H}{\partial t} + \alpha \frac{\partial H}{\partial x} + \beta \frac{\partial H}{\partial y} + \gamma \frac{\partial H}{\partial z} = 0 \tag{3.4}$$

Energy equation

$$\frac{\partial E}{\partial t} + \alpha \frac{\partial E}{\partial x} + \beta \frac{\partial E}{\partial y} + \gamma \frac{\partial E}{\partial z} = \zeta \left(\frac{\partial^2 E}{\partial x^2} + \frac{\partial^2 E}{\partial y^2} + \frac{\partial^2 E}{\partial z^2} \right) + \Delta S \tag{3.5}$$

ζ is the thermal diffusion coefficient, $\zeta = \xi / \rho_{c_p} \cdot c_p$ is the specific heat capacity, ξ is the thermal conductivity and ΔS is the latent heat of condensation.

3.3. Simplification of flow area. The flow field diagram of molten steel from box to gate and roll gap center line during casting and rolling is given (Fig. 3.1). The change of liquid face value in a specific interval is simplified to the constant value of liquid surface by simulation.

After the liquid level in the current tank is fixed, the midpoint of the gap is used as the starting point of the potential field. On the energy surface, the flow of the liquid obeys the Beendeavor formula:

$$p_0 + \rho g l_0 + \frac{1}{2}\rho \beta_0^2 = p_1 + \rho g l_1 + \frac{1}{2}\rho \beta_1^2 \tag{3.6}$$

The liquid metal level is selected at the connection point between the front box and the casting. The pressure p_0 on the liquid surface of the front tank is atmospheric [13]. In this case, when the liquid flows from the flow tank into the front container, the pulsation rate β_0 on the liquid surface is o. In this coordinate system, $\beta_0 = H.P_1$ is the pressure in the flow field and β_1 is the velocity in the flow field. In the numerical simulation of the flow field and temperature field in the twin-roll casting and rolling process, two methods of constant pressure and constant rate can be used for numerical simulation. In the casting and rolling process, when the liquid metal flows into the casting and rolling area from the gate, the speed of the gate inlet is realized by the static pressure formed by the difference in the liquid level of t front groove [14]. Since the liquid metal fills the casting area, the liquid pressure the gate is greater than the air pressure, so the flow rate of the liquid metal at

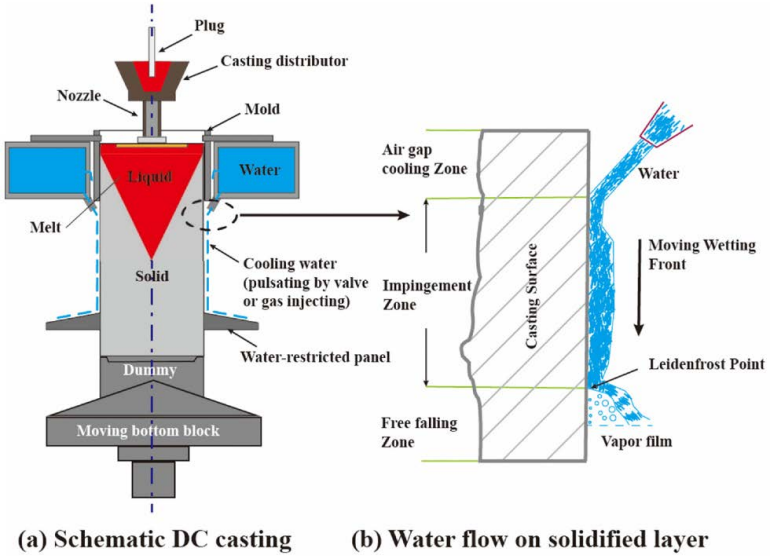

Fig. 3.2: *Schematic diagram of flow area for numerical simulation.*

the gate inlet also changes. The liquid metal in the entire flow field area is driven by constant pressure. In the simulation calculation, the pressure p_1 of the liquid metal at the gate inlet is set as follows:

$$p_1 = p_0 + \rho g l_0 \tag{3.7}$$

When the liquid steel does not slip in the inner surface of the gate and the roll surface, the interface flow rate of the two phases is o. Figure 3.2 shows the digital simulation results of the flow field. In the actual production, the liquid metal flows along the gate to the casting and rolling area, and then through the roll gap's center, the casting and rolling process is realized [15]. The flow and temperature fields of magnesium alloy melt in the continuous casting nozzle and casting and rolling zones were studied.

4. Test results and analysis.

4.1. Rheological properties of magnesium alloys under different vacuum conditions. Fig. 4.1 shows the flow field distribution at the gate plane under different vacuum conditions. When the vacuum degree increases, the rate of pyrolysis products is accelerated, the resistance of liquid propulsion is reduced, the flow rate is accelerated, and the filling time is significantly shortened [16]. In filling a single-track plate, the shape of the flow path shows the central radiation of the inner flow path, and the transition process of mold filling accompanies the transition from the convex arc to the inner flow path. The reason is that the liquid metal will be preferentially filled along the wall of the flow path under negative pressure.

In this process, heat conduction, convection and radiation are carried out between liquid metal and coating, dry sand and non-vaporized foam phase. During gasification mode pyrolysis, a series of physicochemical reactions and material transfer processes occur between molten metal, paint and dry sand. The results show that the Mg-based alloys at different temperatures are dominated by gas phases in different forms at different temperatures. Most gas products are gaseous styrene (about 70%), while small molecules are about 10%. In the process of evaporative molding, the pyrolysis gas formed a significant barrier to the coating layer, the pyrolysis products were discharged under negative pressure, and the pyrolysis products were concentrated in the outer boundary [17]. The accumulation of pyrolysis products at the front end of the flow field inhibits the forward movement of magnesium alloy melt, forming a convex arc shape with the inner gate in the center. With the increase of vacuum degree, the discharge rate of thermal decomposition products at the surface boundary increases significantly, accelerating the filling of the liquid boundary, enhancing the adhesion effect of the wall surface making the flow field's front shape smoother.

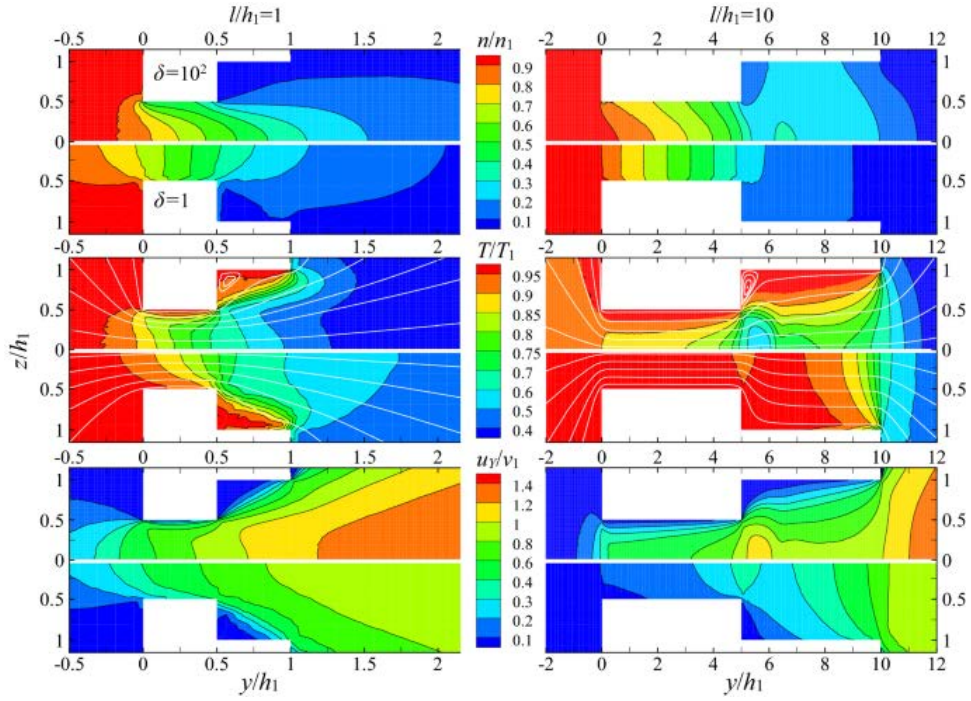

Fig. 4.1: *Flow field distribution of a single plate under different vacuum conditions.*

4.2. Influence of pouring temperature and number of gates on melt structure of MG-base alloy. Fig. 4.2 shows the variation of the shape of the flow field front in a single bottom surface and two channel plates with the pouring temperature when the vacuum degree is 0.02 MPa and the foam density is 0.020 g /cm3, and different pouring temperatures are adopted. The results show that when the liquid metal flows into the sample from the inner gate, the liquid metal forms a raised arc upward, which is roughly symmetric with the gate. When the flow front continues to advance, the liquid metal gradually fills the sample's cross-section, the flow field's curvature decreases during this process, and the movement of the liquid metal tends to be stable [18]. After this, the metal tip progresses in approximately the same pattern until the liquid metal reaches the top of the sample and is filled. The filling shapes of the two materials are not different at different pouring temperatures, but different pouring temperatures greatly influence the filling time, and it decreases with the increase in pouring temperature. With the increase in pouring temperature, the appearance vaporization rate increases, and the escape rate of the pyrolysis product increases under the same vacuum condition, thus reducing the molding time. In the process of filling the mold of the double-layer inner gate, the two liquids are filled with the same curvature, "double peaks," and in the forward process, the two liquids fuse into one in forward process, the bending degree is reduced, and the filling mold is more stable. Compared with a single plate, the double cavity can also reduce the filling time, making the filling process more stable.

4.3. Flow rate of metal melt during casting of lost mold. Fig. 4.3 shows the relationship between the filling rate of magnesium alloy liquid along the flow direction and the flow channel length under different vacuum degrees, pouring temperature and foam concentration [19]. The flow rate is determined by the time difference between the two contact points according to the distance between the two contact points in the flow direction, so the filling rate is the average rate between each contact point. The results show that the flow rate of magnesium increases first and then decreases during the filling process, but over time, the flow rate of magnesium changes continuously. It is necessary to alternate fast and slow to ensure the continuity of filling. A cracking reaction occurs when liquid metals meet under heating conditions, and the cracking product increases the resistance of liquid propulsion, mainly determined by the melt decomposition rate and

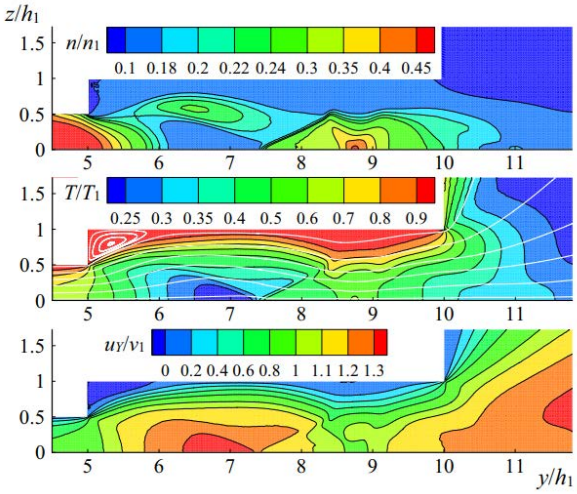

Fig. 4.2: *Flow front morphology of single gate and double gate plate at different pouring temperatures.*

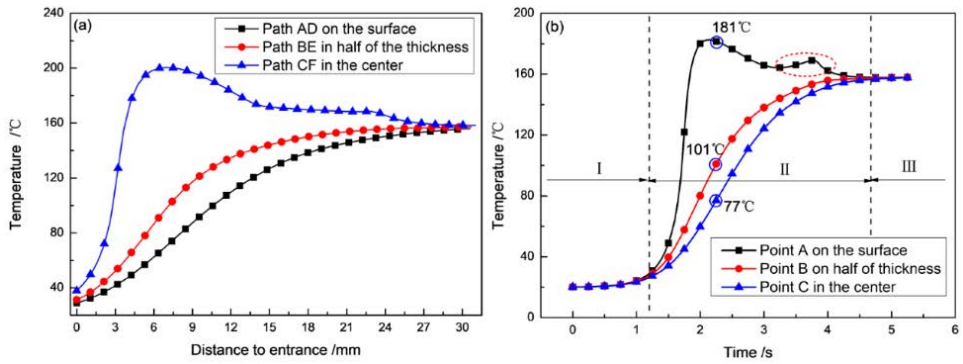

Fig. 4.3: *The relationship between the gate plane sample's filling rate and the flow path length under various processing parameters.*

product discharge range. The thrust force of liquid metal in the filling-blanking mode of liquid magnesium melt is mainly determined by gate pressure and injection volume. The resistance generated during filling is mainly due to the gas and liquid products not being discharged in time. The filling rate of liquid magnesium depends on the relative value of thrust and resistance. The movement rate of liquid magnesium alloy melt in the early casting stage is mainly due to its high gas permeability or negative pressure effect, which reduces the propropulsion resistance of liquid magnesium alloy. At this time, there is a significant gap in the transition layer between the metal melt and the bubble phase. The gap is getting smaller. When the melt flow rate of magnesium alloy is greater than the decomposition rate of the foam phase, the interfacial spacing of melt droplets becomes narrower. The thermal resistance of droplet gas and liquid product increases, and the melt filling rate decreases. At the same time, the heat transfer on the magnesium alloy surface is enhanced with the reduction of the interfacial spacing. At this time, the cracking rate of the morphology is faster than that of the previously reduced liquid melt, so the transition layer increases, the flow resistance decreases, and the filling rate increases again. The velocity of magnesium alloy melt again exceeds the decomposition rate of metal melt. Under different mold filling conditions, the change of void size and resistance in the transition layer can explain

the periodic change in mold filling rate. It is necessary to use different pouring rates to control according to the different flow rates of magnesium alloy melt to ensure the continuous filling of liquid metal. When pouring, the straight gate should be filled. Otherwise, due to the low heat capacity of magnesium alloy wire, it is easy to have the disadvantage of a poor gate. If the injection rate is too high, the appearance of rapid evaporation will occur, and there will be a large amount of gas backflow or lead to magnesium alloy solution leakage from the pouring cup.

5. Conclusion.

1. During vacuum grouting filling, due to the accumulation of products generated by thermal decomposition at the front end of the flow, especially the outer edge, the magnesium alloy solution advances from the inner gate in a convex arc shape. The flow field structure tends to be stable during mold-filling, but wall adhesion will occur when the vacuum degree increases. The filling time is shortened with the increase of pouring temperature and vacuum degree.
2. The filling rate of magnesium alloy is generally from high to low, showing a periodic change during this period.

REFERENCES

[1] Shehata, M. M., El-Hadad, S., Moussa, M. E., & El-Shennawy, M. (2021). The combined effect of cooling slope plate casting and mold vibration on microstructure, hardness and wear behavior of Al–Si alloy (A390). International Journal of Metalcasting, 15(3), 763-779.

[2] Shayan, M., Eghbali, B., & Niroumand, B. (2020). Fabrication of AA2024− TiO2 nanocomposites through stir casting process. Transactions of Nonferrous Metals Society of China, 30(11), 2891-2903.

[3] Javaid, A., & Czerwinski, F. (2021). Progress in twin roll casting of magnesium alloys: A review. Journal of Magnesium and Alloys, 9(2), 362-391.

[4] Wu, G., Wang, C., Sun, M., & Ding, W. (2021). Recent developments and applications on high-performance cast magnesium rare-earth alloys. Journal of Magnesium and Alloys, 9(1), 1-20.

[5] Kumar, A., Rana, R. S., & Purohit, R. (2020). Effect of stirrer design on microstructure of MWCNT and Al alloy by stir casting process. Advances in Materials and Processing Technologies, 6(2), 320-327.

[6] BADIZI, R. M., Parizad, A., Askari-Paykani, M., & Shahverdi, H. R. (2020). Optimization of mechanical properties using D-optimal factorial design of experiment: Electromagnetic stir casting process of A357− SiC nanocomposite. Transactions of Nonferrous Metals Society of China, 30(5), 1183-1194.

[7] Rao, M. S. S., & Kumar, A. (2024). Experimental study and optimization of process parameters for producing semi-solid A392 alloy using vibration-assisted cooling slope process integrated with mould vibration. International Journal of Metalcasting, 18(2), 944-961.

[8] Gurusamy, P., Raj, S. H. K., Bhattacharjee, B., & Bhowmik, A. (2024). Assessment of microstructure and investigation into the mechanical characteristics and machinability of A356 aluminum hybrid composite reinforced with SiCp and MWCNTs fabricated through rotary centrifugal and squeeze casting processes. Silicon, 16(1), 367-382.

[9] Dong, Y. W., Shao, P. F., Guo, X., Xu, B., Yin, C. P., & Tan, Z. Y. (2023). Deformation characterization method of typical double-walled turbine blade structure during casting process. Journal of Iron and Steel Research International, 30(10), 2010-2020.

[10] Nişancı, M. C., & Yurddaş, A. (2020). Compare between the results of the casting simulation and the results of experimental production with calculating the interface heat transfer coefficient of the casting-mold. Celal Bayar University Journal of Science, 16(2), 169-181.

[11] Asano, K., Yamada, H., & Sugimura, S. (2024). Erosion resistance of heat-treated aluminum cast iron to aluminum alloy melt. MATERIALS TRANSACTIONS, 65(5), 534-540.

[12] Kanyo, J. E., Schafföner, S., Uwanyuze, R. S., & Leary, K. S. (2020). An overview of ceramic molds for investment casting of nickel superalloys. Journal of the European Ceramic Society, 40(15), 4955-4973.

[13] Sankhla, A., & Patel, K. M. (2022). Metal matrix composites fabricated by stir casting process–a review. Advances in Materials and Processing Technologies, 8(2), 1270-1291.

[14] Schurmann, D., Glavinić, I., Willers, B., Timmel, K., & Eckert, S. (2020). Impact of the electromagnetic brake position on the flow structure in a slab continuous casting mold: An experimental parameter study. Metallurgical and Materials Transactions B, 51(1), 61-78.

[15] Terwadkar, A. R., Sahasrabuddhe, A. V., & Kulkarni, M. M. (2020). Implementation of Statistical Quality Control Techniques to Minimize the Casting Defects. International Research Journal of Engineering and Technology (IRJET), 7(12), 1533-1544.

[16] Berti, S., Jagus, R. J., Flores, S. K., & González-Martínez, C. (2024). Antimicrobial Edible Starch Films Obtained By Casting and Thermo compression Techniques. Food and Bioprocess Technology, 17(4), 904-916.

[17] Hao, X., Liu, G. H., Wang, Y., Wu, S. P., & Wang, Z. D. (2022). Optimization of investment casting process for K477 superalloy aero-engine turbine nozzle by simulation and experiment. China Foundry, 19(4), 351-358.

[18] Guan, F., Jiang, W., Li, G., Zhu, J., Wang, J., Jie, G., & Fan, Z. (2022). Effect of vibration on interfacial microstructure

and mechanical properties of Mg/Al bimetal prepared by a novel compound casting. Journal of Magnesium and Alloys, 10(8), 2296-2309.
[19] Guo, Z., Jie, J., Liu, S., Liu, J., Yue, S., Zhang, Y., & Li, T. (2020). Solidification characteristics and segregation behavior of Cu-15Ni-8Sn alloy. Metallurgical and Materials Transactions A, 51(3), 1229-1241.

Edited by: Hailong Li
Special issue on: Deep Learning in Healthcare
Received: May 24, 2024
Accepted: Jul 5, 2024